Journal of Radiation Research, Vol. 59, No. 2, 2018, pp. 164–172
doi: 10.1093/jrr/rrx067
Advance Access Publication: 14 December 2017

Dosimetric and clinical effects of interfraction and intrafraction correlation errors during marker-based real-time tumor tracking for liver SBRT

Keita Kurosu[1,2], Iori Sumida[1,*], Osamu Suzuki[1], Hiroya Shiomi[1], Seiichi Ota[2], Keisuke Otani[1], Keisuke Tamari[1], Yuji Seo[1] and Kazuhiko Ogawa[1]

[1]Department of Radiation Oncology, Osaka University Graduate School of Medicine, 2-2 Yamadaoka, Suita, Osaka, 565-0871, Japan
[2]Department of Radiology, Osaka University Hospital, 2-15 Yamadaoka, Suita, Osaka, 565-0871, Japan
*Corresponding author. Department of Radiation Oncology, Osaka University Graduate School of Medicine, Osaka, 565-0871, Japan. Tel: +81-6-6879-3482; Fax: +81-6-6879-3489; Email: sumida@radonc.med.osaka-u.ac.jp
(Received 23 May 2017; revised 13 September 2017; editorial decision 14 October 2017)

ABSTRACT

Correlation model error (*CME*) between the internal target and the external surrogate, and marker–tumor correlation error (*MTCE*) between the tumor and the implanted marker occur during marker-based real-time tumor tracking. The effects of these intrafraction and interfraction errors on the dose coverage in the clinical target volume (*CTV*) and on tumor control probability (*TCP*) for hepatocellular carcinoma (HCC) were evaluated in this study. Eight HCC patients treated with non-isocentric dose delivery by a robotic radiosurgery system were enrolled. The *CMEs* were extracted from the treatment log file, and the *MTCEs* were calculated from the preceding study. The *CMEs* and *MTCEs* were randomly added to each beam's robot position, and the changes in the *TCP* and the 2%, 95% and 99% dose coverage values for the *CTV* (*D2*, *D95* and *D99*) were simulated. The data were statistically analyzed as a function of the *CTV* to planning target volume (*PTV*) margin, the dose fraction and the marker–tumor distance. Significant differences were observed in the majority of the *CTV D2*, *D95* and *D99* values and the *TCP* values. However, a linear regression revealed that Δ*CTV D2*, *D95* and *D99* have a weak correlation with Δ*TCP*. A dose-difference metric would be unable to detect a critical error for tumor control if the coverage changes for the *CTV* and Δ*TCP* were weakly correlated. Because the simulated *TCP*-based parameter determination was based on the dose simulation, including predicted interfraction and intrafraction errors, we concluded that a 95th percentile *TCP*-based parameter determination would be a robust strategy for ensuring tumor control while reducing doses to normal structures.

Keywords: CyberKnife; Synchrony Respiratory Tracking System; stereotactic body radiotherapy; correlation model error; marker–tumor correlation error

INTRODUCTION

Motion management is required for delivering accurate doses to targets that move with respiration [1]. The dynamic movement of radiation beams is a motion management strategy often referred to as real-time tracking. The CyberKnife® G4 robotic radiosurgery system (Accuray Inc., Sunnyvale, CA, USA) integrates the Synchrony® Respiratory Tracking System (SRTS), enabling real-time adjustments with changes in a moving target's positions [2, 3]. Real-time tumor adjustment can be achieved using internal landmarks such as implanted fiducial markers (fiducial/Synchrony) or the lung tumor itself (Xsight Lung™), which is identified using two pairs of X-ray tubes and flat-panel detectors [4, 5]. In marker-based tracking, the internal tumor position is determined by detecting fiducial markers, because a stable correlation between fiducial marker and tumor position is required for reducing the day-to-day tumor displacement [6]. However, fiducial implantation inside a tumor should be avoided in hepatocellular carcinoma (HCC) because of the risk of spreading tumor cells by needle puncture [7]; hence, fiducials are implanted at a certain distance from the tumor. The distance between fiducial marker and the tumor position is not constant

during the treatment period due to the deformation or rotation of fiducials, resulting in a correlation error between the fiducials and the tumor positions. This marker–tumor correlation error (MTCE) is counted as interfraction, but its impact has not been reported.

Tumor tracking by SRTS is performed using a correlation model that relates the position signals from an external surrogate to the internal target position in preparation for the baseline shift or change in breathing pattern [8]. At treatment initiation using SRTS, the fiducial marker location is identified at multiple discrete time points by acquiring orthogonal X-ray images. A linear or quadratic correlation model is then generated by fitting the 3D marker location at different phases of the breathing cycle to simultaneous external optical marker positions attached on the abdomen [9]. This correlation model provides an estimate of the target position from the external marker variable. The estimate is sent to the robotic manipulator; it then dynamically moves the linear accelerator. The correlation model is checked and updated during the treatment by acquiring orthogonal X-ray images; however, residual errors are observed between the predicted and actual target positions [10, 11]. These errors are counted as intrafractions and may result in overdoses and underdoses inside the target through interplay and dose-blurring effects [12].

Stereotactic body radiotherapy (SBRT) has become a major strategy for locally ablative therapy in HCC management because of its high tumoricidal effect [13–15]. However, interfraction and intrafraction errors can be a major problem in SBRT: the small number of fractions can increase the risk of missing the target [16]. The dose coverage change for the clinical target volume (*CTV*) has been evaluated as a predictor for the treatment robustness; however, several reports have indicated a limitation for predicting the resultant tumor control probability (*TCP*) in intensity-modulated radiation therapy [17, 18]. Here, dose simulations were performed to determine the effects of interfraction *MTCE* and intrafraction correlation model error (*CME*) on dose coverage change for the *CTV* and *TCP*. Following the simulation, two topics will be discussed: (i) whether dose coverage change for the CTV is a predictor for ΔTCP in hypofractionated radiation therapy; (ii) whether treatment parameters, such as the *CTV* to planning target volume (*PTV*) margin, dose fraction, marker–tumor distance, and ΔTCP distribution can be correlated.

MATERIALS AND METHODS

Patient population and treatment planning using SRTS

This study was approved by our institutional review board and conducted in accordance with the principles of the Declaration of Helsinki. Eight patients who underwent liver SBRT using SRTS between July 2014 and November 2015 were enrolled in this study. More than a week before the acquisition of treatment planning computed tomography (CT) data, a single fiducial marker (0.75 mm × 5.0 mm Visicoil®, SCETI Medical Labo KK, Tokyo, Japan) was percutaneously implanted around the target under ultrasound or CT guidance. Patients were placed in the supine position using a VacLok™ positioning cushion (CIVCO Medical Solutions, Kalona, IA, USA); CT images with a 1.25-mm slice thickness in exhale breath hold were then scanned. Contrast-enhanced CT was simultaneously acquired to aid target delineation. Radiation oncologists performed gross tumor volume (*GTV*) delineation. No *GTV* to *CTV* margin was added for subclinical extension. In this study, 3- [19] and 5-mm [11] *CTV–PTV* margins were isotropically added to the *CTV*. Treatment plans were created using the MultiPlan® version 4.6.1 (Accuray Inc., Sunnyvale, CA, USA) treatment planning system; the Ray-tracing algorithm using a $0.59 \times 0.59 \times 1.25\text{-mm}^3$ voxel size was the dosing engine. All treatment plans used non-isocentric dose delivery with an IRIS™ variable-aperture collimator. The aperture size was determined for each *CTV–PTV* margin; all sizes from 10 mm to the *PTV* diameter were used. The differences in the conformity index (*CI*) and heterogeneity index (*HI*) between treatment plans with two types of margins were set to a small value, with the intention that a significant difference would not be observed in dose conformity and inhomogeneity at the target. *CI* and *HI* were calculated using the following equations [20]:

$$CI = \frac{V_{RI}}{TV}, \tag{1}$$

$$HI = \frac{I_{max}}{RI}, \tag{2}$$

where V_{RI} is the reference isodose volume, *TV* is the target volume, I_{max} is the maximum isodose in the target, and *RI* is the reference isodose. The treatment time was adjusted to the original plan by considering the actual dose delivery in clinical situations. The isodose covering 95% of the *PTV* was used as the dose prescription, with a biologically effective dose (BED_2) of 70 Gy was less than 30% of normal liver [21].

Correlation model error

The CyberKnife tracking information, such as the output of correlation modeler points and predictor points, is stored in the log files for all treatment fractions [10]. *CME*, the difference between the predicted and actual target positions, was extracted from the log file, and *CMEs* were recorded immediately before the beam deliveries were isolated. The acquisition interval of the X-ray images and the *CME* log file was 45–60 s. In this study, *CME* was considered over the entire treatment session course. The absolute mean, standard deviation (SD), and 95th percentile *CMEs* were calculated in superior–inferior (SI), anterior–posterior (AP), left–right (LR) and 3D radial directions.

Marker–tumor correlation error

Interfraction *MTCEs* depend on the marker–tumor distance [6]. If the marker–tumor distance was <60 mm, the marker-guided set-up was more accurate than the alternative set-up strategies, such as using bony anatomy, a stereotactic body frame, and a diaphragm dome [6]. The systematic and random *MTCEs* were extracted from the data of Seppenwoolde *et al.* [6] because they were presented as *population* SDs, i.e. estimated the errors in an infinite number of patients and fractions. Because the *population* SD does not reflect the real systematic and random error distribution in a hypofractionated treatment, it requires a conversion to a finite number of fractions using the following equations [22]:

$$\sigma_{i\,eff}^2 = \left(1 - \frac{1}{F}\right)\sigma_i^2 \; for \; i \in \{x, y, z\}, \tag{3}$$

and

$$\sum_{i\,eff}^2 = \sum_i^2 + \frac{1}{F}\sigma_i^2 \; for \; i \in \{x, y, z\}, \tag{4}$$

where F is the fraction number, σ is the *population* SD of the random error, and Σ is the *population* SD of the systematic error. The *effective* SD of the random error in F fractionated treatment is denoted as σ_{eff} and that of systematic error as Σ_{eff}. The patient coordinate is based on the supine position: $+X$ indicates the inferior direction; $+Y$ the left direction; and $+Z$ the anterior direction. For dose simulation, because interfraction *MTCE* should be converted to a single input parameter (dose simulation details will be provided later), systematic and random errors vectors were composed based on the following equation, which represents a 'daily' *MTCE*:

$$MTCE_i = \sqrt{\Sigma_{i\,eff}^2 + \sigma_{i\,eff}^2} \; for \; i \in \{x, y, z\}. \tag{5}$$

Dose simulation

The dosimetric effects of intrafraction and interfraction errors were simulated using ShioRIS2.0 (RADLab Co. Ltd., Osaka, Japan) software. For dose simulation, ShioRIS imports SDs of intrafraction and interfraction errors for individual patients, the Digital Imaging and Communications in Medicine–Radiation Therapy (DICOM-RT) dose, the DICOM-RT structure set, a CT image series, and the original treatment plan file (XML format). The intrafraction error was randomly added to each beam's robot position, using a normal distribution with $\sigma =$ CME for the SI, AP and LR directions. The interfraction error was systematically added to each beam's robot position during a single fraction using a normal distribution with $\sigma = MTCE$ of each marker–tumor distance (marker–tumor distance will be detailed later). For a series of treatment plans, the error-included dose distribution was simulated 1000 times to suppress the standard error to within 0.5%. The simulation was performed using the Ray-tracing algorithm with a $0.59 \times 0.59 \times 1.25\text{-mm}^3$ voxel size, similar to the calculation in the MultiPlan. In the case of one [13], three [14] and five [15] practical dose fractions were simulated. The prescribed dose was divided into each fraction; thereby, the number of beams and treatment time were held constant. Regarding the marker–tumor distance, the implanted markers cannot always be proximal to the target because of limitations associated with needle puncture. Therefore, calculated *MTCEs* for the marker–tumor distances of 20, 60 and 100 mm were included in this study to consider the superior and inferior cases for marker-guided set-up. The computational accuracy of ShioRIS has been previously validated [23] for cases in which the mean dose differences from doses calculated by the MultiPlan are <0.5% for percentage depth dose and lateral dose profile.

For this study, the simulated *CTV D2*, *D95* and *D99* (*DX* referring to dose level covering *X*% of target volume) were compared with the original data for various *CTV–PTV* margins, dose fractions, and marker–tumor distances. $\Delta CTV\ D2$, *D95* and *D99* were calculated according to the following equation:

$$\Delta CTV\ DX\ [\%] = \frac{CTV\ DX_{(\text{sim})} - CTV\ DX_{(\text{plan})}}{CTV\ DX_{(\text{plan})}} \times 100, \tag{6}$$

where $CTV\ DX_{(\text{plan})}$ is the dose coverage value in the original treatment plan and $CTV\ DX_{(\text{sim})}$ the dose coverage value in the simulated one. X refers to the percentage coverage for the *CTV*; $X = 2\%$, 95% and 99% were investigated.

TCP calculation

CTV simulated and planned dose–volume histograms were extracted from each setting of *CTV–PTV* margin, dose fraction, and marker–tumor distance, and the *TCP* for HCC was then calculated. We assumed a treatment plan of 36 Gy in three fractions at the 95% border of the *PTV* [14]. The dose regimen was converted for one and five fractions, maintaining a fraction-size equivalent dose (*FED*) of 2 Gy per fraction at 66 Gy, with an α/β ratio of 10 [24]: physical doses were 24 Gy in a single fraction and 43 Gy in five fractions. A two-parameter phenomenological *TCP* model was used for *TCP* calculation, based on a logit expression [25]:

$$TCP\left\{\left((FED_{10}^2)_i,\, v_i\right)\right\} = \prod_{i=1}^{N}\left[\frac{1}{1 + \left(TC\,(FED_{10}^2)_{50}/(FED_{10}^2)_i\right)^{4\gamma 50}}\right]^{v_i}, \tag{7}$$

where

$$\sum_{i=1}^{N} v_i = 1, \tag{8}$$

and

$$FED_{\alpha/\beta}^{fs} \equiv nd\frac{\left(1 + \frac{d}{\alpha/\beta}\right)}{\left(1 + \frac{fs}{\alpha/\beta}\right)} \tag{9}$$

In this expression, the input v_i is the fractional volume that receives a dose level of FED_i; $TCFED_{50}$ is the *FED* required to achieve 50% *TCP*; γ_{50} is the normalized slope of the *TCP* curve at $TCFED_{50}$; and d is the physical dose delivered per fraction at some chosen point of interest. $TCFED_{50} = 53$ Gy and $\gamma_{50} = 2.76$ were used for HCC, and the *FED* was calculated using a linear–quadratic model with an α/β ratio of 10 [26]. ΔTCP was then calculated for each dose simulation, defined as the simulated *TCP* subtracted from that of the original treatment plan.

Statistical analysis

CI and *HI* comparisons based on 3- and 5-mm *CTV–PTV* margins were made using the paired *t*-test or Wilcoxon signed-rank test, depending on sample normality (Shapiro–Wilk test). Dose coverage change comparisons for the *CTV* with two types of *CTV–PTV* margins were made using the paired *t*-test. Similarly, dose coverage change comparisons with different dose fractions and marker–tumor

Table 1. Description of eight study plans enrolled in this study

Plan characteristics	*CTV–PTV* margin of 3 mm	*CTV–PTV* margin of 5 mm
Mean (range) size of *CTV*	8.5 cm^3 (2.2–13.7 cm^3)	
Mean (range) size of *PTV*	16.9 cm^3 (5.5–28.5 cm^3)	24.7 cm^3 (9.8–38.8 cm^3)
Mean (range) of M–T distance	19.9 mm (8.0–43.8 mm)	
Mean (range) of marker amplitude for SI	4.3 mm (1.7–7.1 mm)	
Mean (range) of marker amplitude for AP	4.1 mm (0.6–7.0 mm)	
Mean (range) of marker amplitude for LR	2.4 mm (0.2–4.7 mm)	
Mean (range) of conformity index	1.3 (1.1–2.1)	1.3 (1.1–1.7)
Mean (range) of homogeneity index	1.4 (1.1–1.5)	1.3 (1.2–1.5)
Mean (range) #nodes	35 (15–46)	33 (14–67)
Mean (range) #beams	67 (48–95)	74 (52–125)
Median (range) size of cone	25 mm (10–40 mm)	25 mm (10–60 mm)
Mean (range) of treatment time	35 min (31–40 min)	35 min (30–40 min)

M–T distance = marker–tumor distance, SI = superior–inferior, AP = anterior–posterior, LR = left–right.

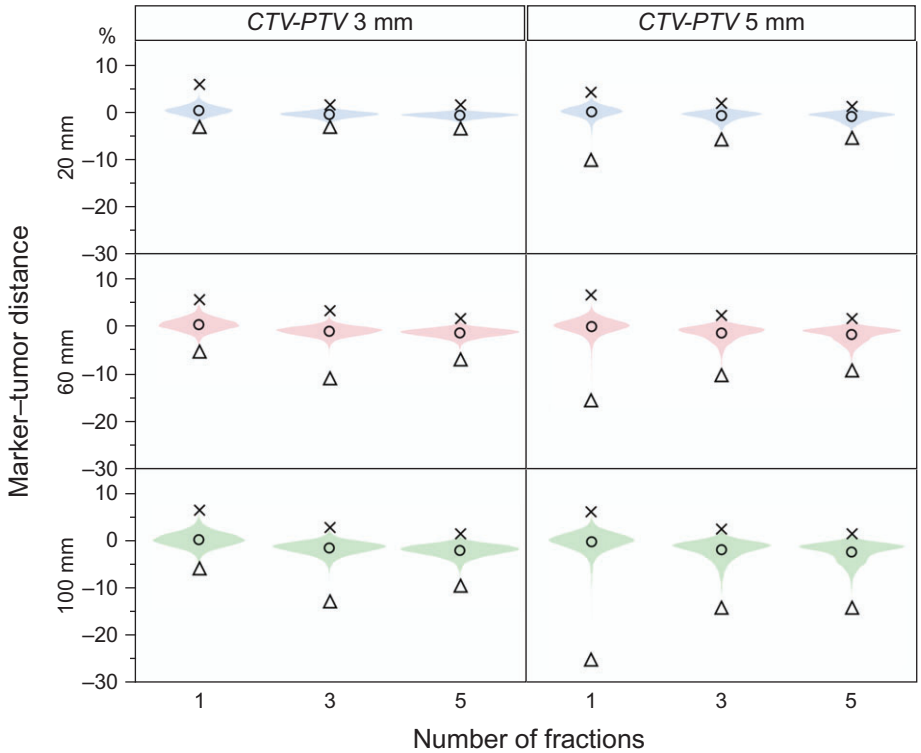

Fig. 1. Change in *CTV D2* depending on marker–tumor distance, *CTV–PTV* margin, and dose fraction. The vertical axis represents the dose coverage change for the *CTV* between planned and simulated. Circle = mean dose coverage change, cross: maximum increase in dose coverage change, triangle = maximum decrease in dose coverage change, *CTV* = clinical target volume, *PTV* = planning target volume.

distances were made using the Tukey–Kramer test. Multiple regression analysis was performed to determine whether the *CTV–PTV* margin, dose fraction, and marker–tumor distance were independently associated with Δ*CTV D2*, *D95*, *D99* and Δ*TCP*. To predict Δ*CTV D2*, *D95*, *D99* and Δ*TCP* distributions, regression analyses were performed on 95th percentile values. A linear regression was also performed between Δ*TCP* and Δ*CTV D2*, *D95* and *D99*. All statistical analyses used JMP® 11 statistical software (SAS Institute Inc., Cary, NC, USA). $P < 0.05$ indicated statistical significance.

RESULTS

Table 1 describes the treatment plan characteristics with 3- and 5-mm *CTV–PTV* margins. No significant differences in *CI* and *HI* were observed between the two margin sizes ($P = 0.563$, $P = 0.936$). For the SI, AP, LR and 3D radial directions, the absolute means ± SDs of *CMEs* were 0.7 ± 0.6 mm, 0.6 ± 0.5 mm, 0.5 ± 0.5 mm and 1.2 ± 0.7 mm, respectively, and the 95th percentile *CMEs* were 1.9 mm, 1.6 mm, 1.5 mm and 2.6 mm, respectively. The 95th percentile *MTCEs* were 5.6 mm, 6.0 mm and 6.1 mm for marker–tumor distances of 20 mm, 60 mm and 100 mm, respectively.

Figures 1–3 present dosimetric effects of *MTCE* and *CME* on the dose coverage for the CTV. Significant differences in dose coverage between CTV–PTV margins (3 mm vs 5 mm) and dose fractions (1 fr vs 3 fr, 1 fr vs 5 fr, and 3 fr vs 5 fr) were observed for all combinations of parameter settings ($P < 0.001$). Similarly, significant differences were observed between pairs of marker–tumor distances (20 mm vs 60 mm, 20 mm vs 100 mm, and 60 mm vs 100 mm), except for *CTV D2* [20 mm vs 60 mm ($P = 0.507$) and 20 mm vs 100 mm ($P = 0.131$)] for a single fraction and a 3-mm *CTV–PTV* margin.

Figure 4 shows the distributions in Δ*TCP*. Significant differences were observed in the *CTV–PTV* margin and marker–tumor distances for all combinations of parameter settings ($P < 0.001$), resulting in the same trend as that for the dose coverage change for the *CTV*. Similarly, significant differences were observed between pairs of dose fractions, except for 3 fr vs 5 fr with a marker–tumor distance of 20 mm and 100 mm, for a 5-mm *CTV–PTV* margin.

Multiple regression analysis showed that the *CTV–PTV* margin, dose fraction, and marker–tumor distance were significant factors associated with 95th percentile Δ*CTV D2*, *D95*, *D99* and Δ*TCP*. Table 2 summarizes the regression analyses results. The most effective factor for suppressing the 95th percentile Δ*CTV D2*, *D95* and *D99* and Δ*TCP* was the *CTV–PTV* margin ($P < 0.001$), followed by the dose fraction ($P < 0.001$) and the marker–tumor distance ($P < 0.001$). A linear regression disclosed that Δ*CTV D2*, *D95* and *D99* have a weak correlation with Δ*TCP*. The contribution ratios (R^2) were 0.00, 0.52 and 0.48 for Δ*CTV D2*, *D95* and *D99* dose coverages, respectively.

DISCUSSION

Although we focused on marker-based SRTS for the CyberKnife system, the *MTCE* will also occur in internal fiducial–based

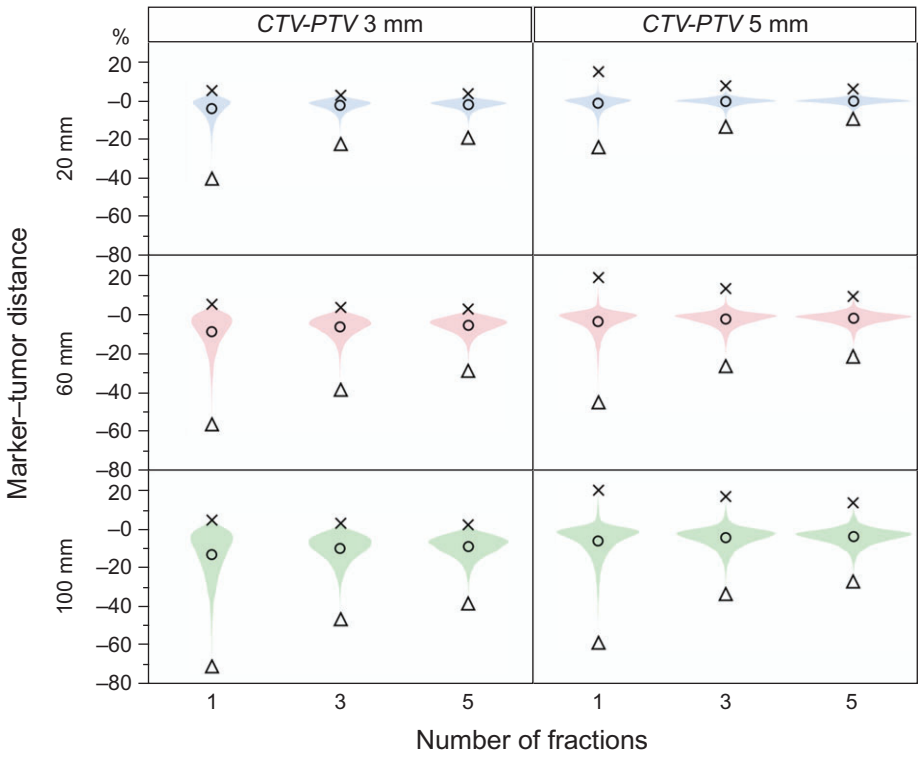

Fig. 2. Change in *CTV D95* depending on marker–tumor distance, *CTV–PTV* margin, and dose fraction. The vertical axis represents the dose coverage change for the *CTV* between planned and simulated. Circle = mean dose coverage change, cross = maximum increase in dose coverage change, triangle = maximum decrease in dose coverage change.

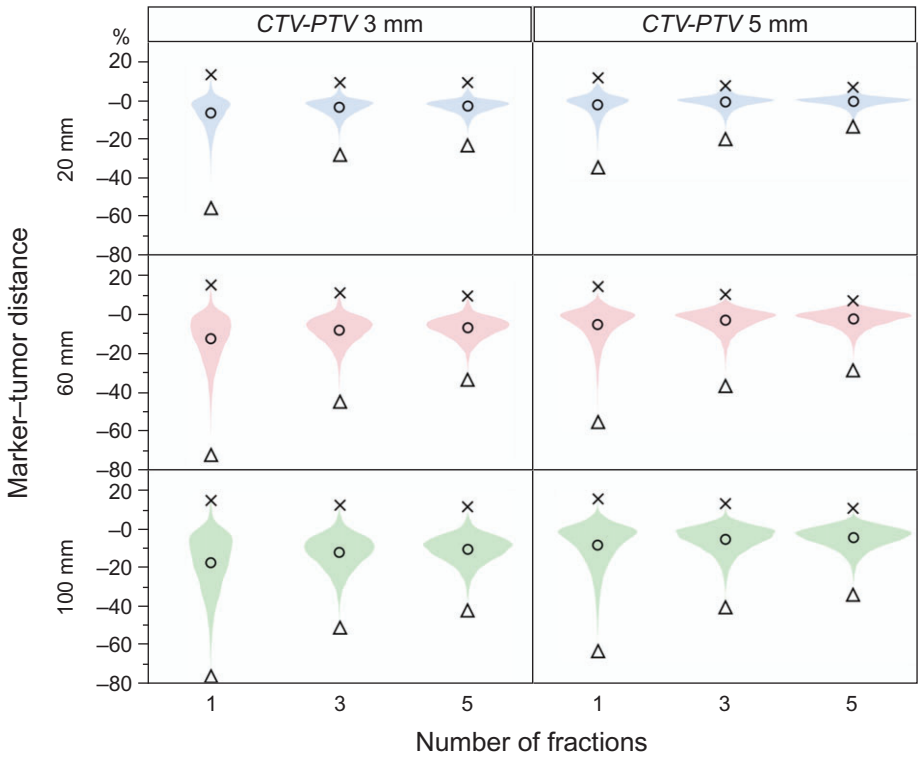

Fig. 3. Change in CTV *D99* depending on marker–tumor distance, CTV–PTV margin, and dose fraction. The vertical axis represents the dose coverage change for the *CTV* between planned and simulated. Circle = mean dose coverage change = cross = maximum increase in dose coverage change, triangle = maximum decrease in dose coverage change.

treatment using a linear accelerator, such as respiratory-gated radiotherapy or Calypso® extracranial tracking system (Varian Medical Systems, Palo Alto, CA, USA). This study revealed *MTCE* and *CME* effects on Δ*CTV D2*, *D95*, *D99* and Δ*TCP* for HCC. At first, additional dose simulation showed that the mean ± SD of Δ*PTV D2*, *D95* and *D99* with a 5-mm *CTV–PTV* margin, five fractions, and a 20-mm marker–tumor distance were −1.1% ± 0.8%, −2.5% ± 2.5% and −2.4% ± 4.4%, respectively. The dosimetric and clinical effects were simulated with different fractionations, but the same planning technique was used for this study. Because the biological effect on the surrounding normal structures was changed as a function of dose fraction, as with that in *TCP*, the planning strategy would differ by fractionations. Thus, this study was limited with regard to normal tissue complications.

Significant differences were found in Δ*CTV D2*, *D95* and *D99* as a function of the *CTV–PTV* margin, dose fractionation, and marker–tumor distance. Multiple regression analysis revealed that margin expansion is the most effective way to improve dose delivery robustness. However, an expansion of the *CTV–PTV* margin inevitably increases the doses to normal structures [27]. In liver radiotherapy, it is difficult to deliver an adequate dose to the *CTV* without causing radiation-induced liver disease (RILD). Decreasing the irradiated normal liver volume is effective at limiting RILD because RILD is associated with the mean liver dose [28]. However, a consensus setting for the *CTV–PTV* margin and dose fractionation has not yet been determined for liver malignancies using SRTS. Temporospatial optimization is a motion-adaptive treatment planning system that enables robust dose delivery to a moving target without the *CTV–PTV* margin [27, 29]. In this optimization, the dose deposition is calculated by the convolution of beamlet fluence with a probability density describing the motion of the pencil beam relative to the target. If the beam is optimized by convolution with a normal *MTCE* and *CME* distribution, the dose to the normal liver will decrease while maintaining the dose to target.

As reported in *ICRU Report 24*, the dose to the target should be kept within 5% of the prescribed dose in 3D conformal radiation therapy to avoid reducing the tumoricidal effect [30]. The dose coverage in the *CTV*, such as *D2*, *D95* and *D99*, were affected by interfraction and intrafraction errors, interplay effect, and dose blurring [12, 16], resulting in >5% errors in the *CTV D95* mean dose in some parameter settings. Nevertheless, the majority of mean Δ*TCPs* were <5%. The relationships between Δ*TCP* and Δ*CTV D2*, *D95* and *D99* were determined, but weak correlations were observed. Our dose simulation depicted a similar result to that of Garcia-Romero *et al.* due to the insensitivity of Δ*CTV D2*, *D95* and *D99* to Δ*TCP* [17]. A dose-difference metric was limited in its ability to predict the clinical outcome because the relationship between the dose coverage change in the *CTV* and Δ*TCP* is governed by the local slope of the *TCP* curve [18]. Meanwhile, multiple regression analysis disclosed that the *CTV–PTV* margin, dose fractionation, and marker–tumor distance were effective predictors for 95th percentile Δ*TCP*. The regression formula would be useful in predicting

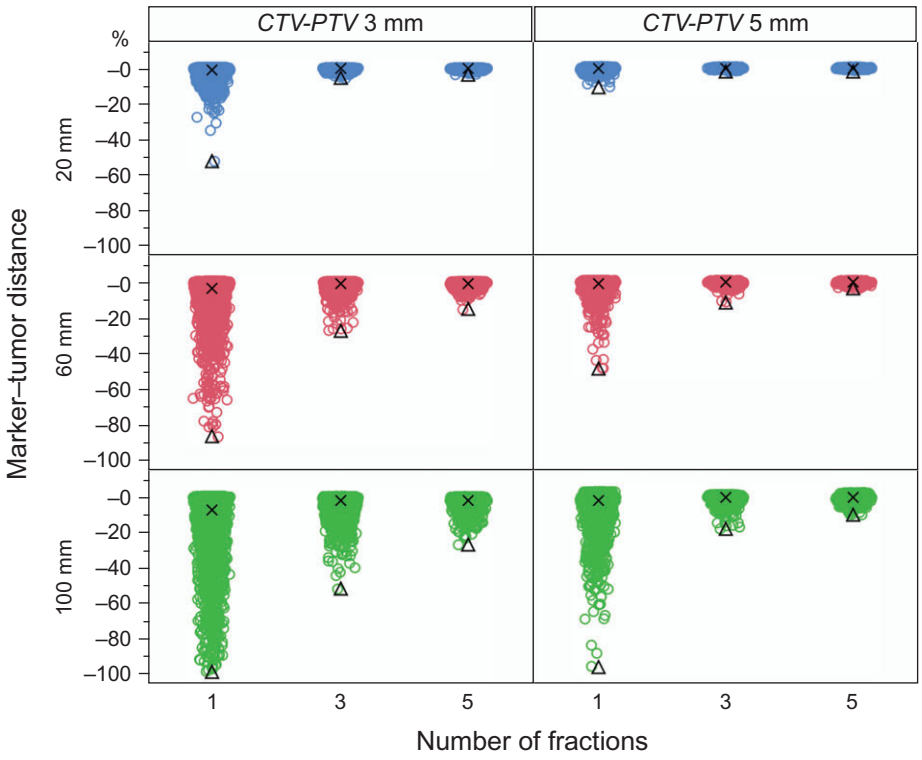

Fig. 4. Distribution in Δ*TCP* of HCC depending on marker–tumor distance, *CTV–PTV* margin, and dose fraction. The vertical axis represents the Δ*TCP* between planned and simulated. Cross = mean Δ*TCP*, triangle = maximum decrease in Δ*TCP*.

the Δ*TCP* distribution with setting parameters. Thus, a 95th percentile *TCP*-based parameter determination would promise robust tumor control because this study has integrated the potential errors occurring during liver SBRT [6, 10, 11] into dose simulation.

This study simulated the dosimetric and clinical effects of interfraction and intrafraction errors from *MTCE* and *CME*, but none of the robotic tracking error, rotational error, or prediction error were included in dose simulations. A report from Task Group No. 135 of the American Association of Physicists in Medicine stated that the overall tracking error must be <1.5 mm for SRTS treatment [31]. In non-isocentric dose delivery, the tracking error of each beam may affect the covered dose in the *CTV* and the *TCP* because a multidirectional beam is used to create the confined dose distribution. Beam-by-beam tracking errors can be quantified using a webcam and a calibrated grid, resulting in <2 mm of beam-by-beam tracking error in sinusoidal breathing cycle [32]. Therefore, a more accurate prediction will be achieved by incorporating each beam's institutional tracking error into dose simulations.

The preceding study calculated *MTCE* by marker registration between the planning and treatment CT scans [6]. They used gold seeds (5 mm long and 1 mm diameter) for marker registration, which we did not. If we had used longer markers than the gold seeds, certain interfraction errors might have been observed in marker registration due to the rotation or deformation of the fiducials; hence, this would limit the direct application of the published data to this study. However, because the longitudinal length of Visicoil was the same and the diameter was comparable with that of the gold seeds, we considered that Seppenwoolde *et al.*'s data [6] could be comparable with our data, even though a different fiducial marker type was used.

This study used a single fiducial marker to perform liver SBRT using SRTS; hence, no rotational information was obtained during treatment. A preceding study revealed that rigid-body liver rotation was <2.0° for roll, pitch and yaw directions [33]. Another study investigated the dosimetric effect of rotational tracking error, but there was no significant correlation between rotational error and dose coverage change for the *CTV* [34]. That study also revealed that the prediction error (the difference between the estimated target position 115 ms later and the actual position) was in submillimeters and resulted in no significance change to the dose coverage for the *CTV* [34]. Thus, although our results were limited in analysis of rotational and prediction errors, the dosimetric and clinical effects from these errors were considered to be small.

Dose-difference metrics would be unable to detect a critical error level for tumor control if the dose coverage change for the *CTV* and Δ*TCP* were weakly correlated [17], because there were no predictors for the resultant *TCP*. This scenario would be mainly observed in stereotactic radiotherapy because the technique concentrates a high dose on the target in a small number of fractions, which boosts *TCP* toward a flat region of the *TCP* curve. There by,

Table 2. Multiple regression analysis of the effects of *MTCE* and *CME* on 95th percentile Δ*CTV D2*, *D95*, *D99* and Δ*TCP* based on *CTV–PTV* margins, dose fractions, and marker–tumor distances

Index	Variable	Coefficient	Standard error	*P*-value
D2 ($R^2 = 0.89$)	Segment	2.11	0.58	<0.01
	PTV margin	−0.66	0.12	<0.001
	Fraction	−0.36	0.07	<0.001
	M−T distance	−0.03	0.00	<0.001
D95 ($R^2 = 0.91$)	Segment	−27.05	3.14	<0.001
	PTV margin	3.72	0.64	<0.001
	Fraction	2.53	0.39	<0.001
	M−T distance	−0.16	0.02	<0.001
D99 ($R^2 = 0.91$)	Segment	−35.33	3.82	<0.001
	PTV margin	4.14	0.78	<0.001
	Fraction	3.56	0.48	<0.001
	M−T distance	−0.19	0.02	<0.001
Δ*TCP* ($R^2 = 0.84$)	Segment	−11.15	8.19	<0.001
	PTV margin	7.83	1.68	<0.001
	Fraction	4.47	1.03	<0.001
	M−T distance	−0.29	0.05	<0.001

Linear regressions were performed on the Δ*CTV D2*, *D95*, and *D99*, while logistic regression was performed on the Δ*TCP*. The scale of *CTV–PTV* margin and marker–tumor distance is presented in millimeters. M–T distance = marker–tumor distance, R^2 = contribution ratio.

the margin estimation for encompassing 95% of the total uncertainty [35], or limiting the dose difference to the target to <5% of the prescription dose [30], may lead to overcompensating for tumor control. In this study, we propose a 95th percentile *TCP*-based parameter determination as a robust tumor control strategy. As this approach would optimize the *CTV–PTV* margin and dose fractionation, satisfying the institutional clinical goal, the doses to surrounding structures (such as the duodenum, bowel and normal liver) could be appropriately controlled [36].

CONCLUSIONS

Through the simulation of the effects of interfraction *MTCE* and intrafraction *CME* on dose coverage change for the *CTV* and on *TCP*, we determined correlations between Δ*CTV* and Δ*TCP*, and between Δ*TCP* distribution and treatment parameters. Δ*CTV D2*, *D95* and *D99* have a weak correlation with Δ*TCP* in hypofractionated radiation therapy, so it was concluded that the dose-difference metric was not able to detect a critical error level for tumor control. However, the treatment parameters were predictive of the Δ*TCP* distribution. Because the simulated *TCP*-based parameter determination was based on the dose simulation, including the predicted interfraction and intrafraction errors, we concluded that a 95th percentile TCP -based parameter determination would be a robust strategy for ensuring tumor control, while reducing doses to normal structures.

CONFLICT OF INTEREST

HS is a member of the company at RADLab Co. Ltd.

FUNDING

This work was supported by a grant from the Japan Society for the Promotion of Science (JSPS) KAKENHI [Grant Number JP16K19230].

REFERENCES

1. Korreman SS. Motion in radiotherapy: photon therapy. *Phys Med Biol* 2012;57:R161–91.
2. Cho B, Suh Y, Dieterich S et al. A monoscopic method for real-time tumour tracking using combined occasional x-ray imaging and continuous respiratory monitoring. *Phys Med Biol* 2008;53:2837–55.
3. Seppenwoolde Y, Berbeco RI, Nishioka S et al. Accuracy of tumor motion compensation algorithm from a robotic respiratory tracking system: a simulation study. *Med Phys* 2007;34:2774–84.

4. Seppenwoolde Y, Shirato H, Kitamura K et al. Precise and real-time measurement of 3D tumor motion in lung due to breathing and heartbeat, measured during radiotherapy. *Int J Radiat Oncol Biol Phys* 2002;53:822–34.
5. Shirato H, Seppenwoolde Y, Kitamura K et al. Intrafractional tumor motion: lung and liver. *Semin Radiat Oncol* 2004;14: 10–8.
6. Seppenwoolde Y, Wunderink W, Wunderink-van Veen SR et al. Treatment precision of image-guided liver SBRT using implanted fiducial markers depends on marker–tumour distance. *Phys Med Biol* 2011;56:5445–68.
7. Llovet JM, Vilana R, Brú C et al. Increased risk of tumor seeding after percutaneous radiofrequency ablation for single hepatocellular carcinoma. *Hepatology* 2001;33:1124–9.
8. Murphy MJ. Tracking moving organs in real time. *Semin Radiat Oncol* 2004;14:91–100.
9. Sayeh S, Wang J, Main WT et al. Respiratory motion tracking for robotic radiosurgery. In: *Treating Tumors that Move with Respiration*, 1st edn. Heidelberg, Germany: Springer-Verlag, 2007.
10. Pepin EW, Wu H, Zhang Y et al. Correlation and prediction uncertainties in the CyberKnife Synchrony respiratory tracking system. *Med Phys* 2011;38:4036–44.
11. Winter JD, Wong R, Swaminath A et al. Accuracy of robotic radiosurgical liver treatment throughout the respiratory cycle. *Int J Radiat Oncol Biol Phys* 2015;93:916–24.
12. Bortfeld T, Jiang SB, Rietzel E. Effects of motion on the total dose distribution. *Semin Radiat Oncol* 2004;14:41–51.
13. Goodman KA, Wiegner EA, Maturen KE et al. Dose-escalation study of single-fraction stereotactic body radiotherapy for liver malignancies. *Int J Radiat Oncol Biol Phys* 2010;78:486–93.
14. Kwon JH, Bae SH, Kim JY et al. Long-term effect of stereotactic body radiation therapy for primary hepatocellular carcinoma ineligible for local ablation therapy or surgical resection. Stereotactic radiotherapy for liver cancer. *BMC Cancer* 2010;10: 475.
15. Huang WY, Jen YM, Lee MS et al. Stereotactic body radiation therapy in recurrent hepatocellular carcinoma. *Int J Radiat Oncol Biol Phys* 2012;84:355–61.
16. Bortfeld T, Jokivarsi K, Goitein M et al. Effects of intra-fraction motion on IMRT dose delivery: statistical analysis and simulation. *Phys Med Biol* 2002;47:2203–20.
17. Garcia-Romero A, Hernandez-Vitoria A, Millan-Cebrian E et al. On the new metrics for IMRT QA verification. *Med Phys* 2016; 43:6058–71.
18. Zhen H, Nelms BE, Tomé WA. On the use of biomathematical models in patient-specific IMRT dose QA. *Med Phys* 2013;40: 071702.
19. Dewas S, Bibault JE, Mirabel X et al. Prognostic factors affecting local control of hepatic tumors treated by stereotactic body radation therapy. *Radiat Oncol* 2012;7:166.
20. Feuvret L, Noël G, Mazeron JJ et al. Conformity index: a review. *Int J Radiat Oncol Biol Phys* 2006;64:333–42.
21. Doi H, Shiomi H, Masai N et al. Threshold doses and prediction of visually apparent liver dysfunction after stereotactic body radiation therapy in cirrhotic and normal livers using magnetic resonance imaging. *J Radiat Res* 2016;57:294–300.
22. de Boer HC, Heijmen BJ. A protocol for the reduction of systematic patient setup errors with minimal portal imaging workload. *Int J Radiat Oncol Biol Phys* 2001;50:1350–65.
23. Kurosu K, Sumida I, Shiomi H et al. A robust measurement point for dose verification in delivery quality assurance for robotic radiosurgery system. *J Radiat Res* 2017;58:378–85.
24. Tomé WA, Fenwick JD. Analysis of radiaiton-induced liver disease using the Lyman NTCP model: in regard to Dawson *et al.* IJROBP 2002;53:810–21. *Int J Radiat Oncol Biol Phys* 2004;58: 1318–9; author reply 1319–20.
25. Kim Y, Tomé WA. Risk-adaptive optimization: selective boosting of high-risk tumor subvolumes. *Int J Radiat Oncol Biol Phys* 2006;66:1528–42.
26. Lausch A, Sinclair K, Lock M et al. Determination and comparison of radiotherapy dose responses for hepatocellular carcinoma and metastatic colorectal liver tumours. *Br J Radiol* 2013;86: 20130147.
27. Trofimov A, Rietzel E, Lu HM et al. Temporo-spatial IMRT optimization: concepts, implementation and initial results. *Phys Med Biol* 2005;50:2779–98.
28. Dawson LA, Ten Haken RK, Lawrence TS Partial irradiation of the liver. *Semin Radiat Oncol* 2001;11:240–6.
29. Chan TC, Tsitsiklis JN, Bortfeld T. Optimal margin and edge-enhanced intensity maps in the presence of motion and uncertainty. *Phys Med Biol* 2010;55:515–33.
30. ICRU. Determination of absorbed dose in a patient irradiated by beams of X or gamma rays in radiotherapy procedures. *ICRU Report 24*. International Comission on Radiation Units and Measurements, Bethesda, MD, 1976.
31. Dieterich S, Cavedon C, Chuang CF et al. Report of AAPM TG 135: quality assurance for robotic radiosurgery. *Med Phys* 2011;38:2914–36.
32. Sumida I, Shiomi H, Higashinaka N et al. Evaluation of tracking accuracy of the CyberKnife system using a webcam and printed calibrated grid. *J Appl Clin Med Phys* 2016;17:74–84.
33. Xu Q, Hanna G, Grimm J et al. Quantifying rigid and nonrigid motion of liver tumors during stereotactic body radiation therapy. *Int J Radiat Oncol Biol Phys* 2014;90:94–101.
34. Chan M, Grehn M, Cremers F et al. Dosimetric implications of residual tracking errors during robotic SBRT of liver metastases. *Int J Radiat Oncol Biol Phys* 2017;97:839–48.
35. Floriano A, García R, Moreno R et al. Retrospective evaluation of CTV to PTV margins using CyberKnife in patients with thoracic tumors. *J Appl Clin Med Phys* 2014;15:59–72.
36. Molinelli S, Pooter J, Romero AM et al. Simultaneous tumour dose escalation and liver sparing in stereotactic body radiation therapy (SBRT) for liver tumours due to CTV-to-PTV margin reduction. *Radiother Oncol* 2008;87:432–8.